ENGINEERING TRIPOS PART IIA 2004

Solutions to Module 3C2
Materials Process Modelling and Failure Analysis
Principal Assessor: Dr M P F Sutcliffe
Second Assessor: Dr C Y Barlow

Engineering Tripos Part IIA: Module 3C2
Manufacturing Engineering Tripos Part I: Paper P4B
Materials process modelling and failure analysis
CRIB - 2004

1. (a) (i) Corrosion will be expected at the following points:
Between brass bolts and steel bars (bimetallic corrosion)
Tack welds; underneath broken paint layer (crevice corrosion);
Twisted (work-hardened) steel wire in contact with mild steel (differential energy corrosion)
At base of posts (crevice corrosion - also see (ii))

In all these cases, the corrosion takes place by anodic dissolution of iron:

$$Fe \Rightarrow Fe^{2+} + 2e^-$$

The usual cathodic process is

$$O_2 + 2H_2O + 4e^- \Rightarrow 4(OH)^-$$

and rust forms by the combination of the two electrode processes

$$2(OH)^- + Fe^{2+} \Rightarrow Fe(OH)_2$$

Iron and brass in contact (bimetallic corrosion)
Iron is more reactive (more electronegative) than brass, so the brass bolts will act as cathodic sites and the iron immediately adjacent to these will become the anode and dissolve.

Tack welds, broken paint layer (crevice corrosion: differential aeration effect)
The areas where the two steel bars are joined are open to the environment (since the discontinuous tack welds do not offer any protection), and in normal UK conditions will contain pooled water.

The cathode process needs oxygen to work, and relies on oxygen gas dissolved in the water. The steel divides itself up into anodic regions and cathodic regions according to how much oxygen there is. The oxygen levels are highest close to the surface of the water, and the lowest oxygen levels are deep inside cracks and crevices. This means that steels are particularly liable to form deep cracks as a result of the presence of water, because once a crack has formed corrosion (anode process) will take place at the crack tip.

A scratch in a paint film provides another opportunity for differential aeration: the bare metal exposed at the scratch is oxygen-rich; the metal just under the edges of the paint film is starved of oxygen, becomes the anode, and dissolves, tunnelling ever deeper under the paint. Rust forming between these two areas helps to lift off the paint film, forming the commonly observed blisters.

Differential energy corrosion (twists of mild steel wire)
The high dislocation density resulting from the work-hardening (twisting of the wire) will give a local increase in stored elastic strain energy in the metal; an anode region will form here. These areas will dissolve, with adjacent regions forming cathodes.

1 (a) (ii) Base of posts (Acid attack: crevice corrosion aggravated by dogs)
Dogs have a tendency to create wet and acid conditions around the bases of posts (increased concentration of H^+). There are often cracks between the iron and the concrete, so allowing pooling of liquid. The iron dissolves using the same anode process as before:

$$Fe \Rightarrow Fe^{2+} + 2e^-$$

The anode process is now different:

$$2H^+ + 2e^- \Rightarrow H_2(gas)$$

Rust may still form, but now uses the small amounts of $(OH)^-$ naturally present in the water. This is not part of the corrosion process, so is not rate-limiting.

$$2(OH)^- + Fe^{2+} \Rightarrow Fe(OH)_2$$

1. (cont)

1 (b) (i)Benefits of microstructural models:
- greater physical understanding of processes (giving a scientific rather than purely empirical basis for improvements in process conditions or control algorithms, or development of new alloys)
- failure analysis (was processing at fault, or product usage? the microstructure can provide vital clues)
- guaranteed microstructure as well as properties)
- potential for "through-process modelling", connecting microstructure evolution through multi-stage manufacturing processes

1 (b) (ii) The term "internal state variable" is used to describe microstructural parameters which can actually be measured (at least in principle). In practice the microstructural state may be inferred by some form of "remote sensing" (hardness, resistivity, X-ray etc). Differential evolution laws for the state variables are integrated over the thermal history, and microstructural-property relationships used to predict the consequent changes in properties (such as strength).

Single state variable models exist for: grain growth (change in average grain size) precipitation, and dissolution of precipitates (characterised by volume fraction of precipitates).

The advantage of a single state variable model is that the evolution law may be *isokinetic* (i.e. the state variable and temperature dependencies in the law are separable):

$$\frac{dS_1}{dt} = \frac{F(S_1)}{t^*(T)}$$ where t*(T) is a function capturing the temperature-dependence of the problem (i.e. always incorporating $\exp(-Q/RT)$).

In this case, the equation can be integrated in one step over the thermal cycle, $T(t)$, to give the final microstructural state:

$$\int \frac{dS_1}{G(S_1)} = \int \frac{dt}{t^*(T)}$$

This is the *kinetic strength* integral – i.e. a measure of the extent of the diffusion-controlled transformation during a thermal cycle.

[The corrosion part of the question was generally well answered. Equations for the various processes were not as accurate as might be expected. Rather vague answers for the benefits of microstructural models and only a relatively small minority appreciated the advantage of deriving a kinetic strength integral.]

2. (a)
Model:
Dimensionality of heat flow (1D, 2D, axisymmetric or 3D); mesh density (number of elements, or graded mesh); element type and shape; linear or higher order elements.

Data:
Input data: thermal properties (conductivity, density, specific heat; or diffusivity combining all three for a transient problem); boundary conditions (heat transfer conditions); initial temperature, and temperature of quenching medium.

Validation data: temperature measurements for validating the results.

2 (b) (i) Semi-infinite bar; sides insulated, so 1D heat flow along bar; perfect heat transfer at the quenched end ($T = T_0$ for $x=0$, $T>0$); constant thermal properties (diffusivity).

2 (b) (ii) From the databook:

$$\frac{d}{dX}[erf(X)] = \frac{2}{\sqrt{\pi}}\exp(-X^2)$$

$$\frac{dX}{dt} = \frac{d}{dt}\left(\frac{x}{2\sqrt{at}}\right) = -\frac{xt^{-3/2}}{4\sqrt{a}} = -\frac{X}{2t}$$

$$T(x,t) = T_0 + (T_1 - T_0)\,erf(X)$$

$$\frac{\partial T}{\partial t} = (T_1 - T_0)\frac{dX}{dt}\frac{d}{dX}[erf(X)] = -\frac{(T_1 - T_0)X}{t\sqrt{\pi}}\exp\left(-X^2\right)$$

Using the approximation: $erf(X) \approx X$, valid for $X < 0.5$, i.e. $T < (T_1 + T_0)/2$

$$\frac{T - T_0}{T_1 - T_0} = erf(X) \approx X$$

and the above expression is still appropriate.

[To eliminate t from this expression for a given reference temperature T, $\frac{T - T_0}{T_1 - T_0}$ = constant,

so X = constant (call this C). $\frac{\partial T}{\partial t} \approx -\frac{(T_1 - T_0)}{\sqrt{\pi}}\left(\frac{C}{t}\right)\exp\left(-C^2\right)$

$\left(\frac{1}{t}\right) \approx \frac{C^2 4a}{x^2}$, (as X = C) $\frac{\partial T}{\partial t} \approx -\frac{(T - T_0)}{\sqrt{\pi}}\left(\frac{C^2\,4\,a}{x^2}\right)\exp\left(-C^2\right)$]

2 (b) (iii) For the temperatures given: $\frac{T - T_0}{T_1 - T_0} = \frac{500-20}{1000-20} = 0.49 = X$

$$t = \frac{x^2}{4aX^2} = 2.17s\,; \quad \frac{\partial T}{\partial t} = -\frac{(T_1 - T_0)X}{t\sqrt{\pi}}\exp\left(-X^2\right) = 98K/s$$

[Alternatively could have got this result by using the equation inside the square brackets above]

2 (c) In the experiment and FE model the length of the bar is specified, while the analytical solution is for a semi-infinite bar. Hence the heat content is fixed for the first cases, but there is an infinite remote heat source in the latter. Near the quenched end, the effect of finite length is not significant (at least in the early stages of cooling), as it takes time for heat to conduct along the bar. In the later stages of cooling however, the analytical solution predicts a much higher temperature, since heat continues to enter the model bar at the end remote from the quench. Moreover the analytical model neglects cooling along the sides. Cooling times are therefore significantly over-estimated.

[Too often the need for good input data and validation was left off the answer to the first part. The straightforward maths of (b)(ii) was normally well done, but using this result to derive the cooling rate in (b)(iii) was less efficient (perhaps due to the structure of this part of the question, which in retrospect was a little confusing - it would have been better to ask for the result at the end of (b)(ii) in terms of x rather than t). The final part was often answered in rather vague terms, without pinning down the critical aspects of the infinite versus finite heat flow problems and the loss along the sides.]

3. (a)

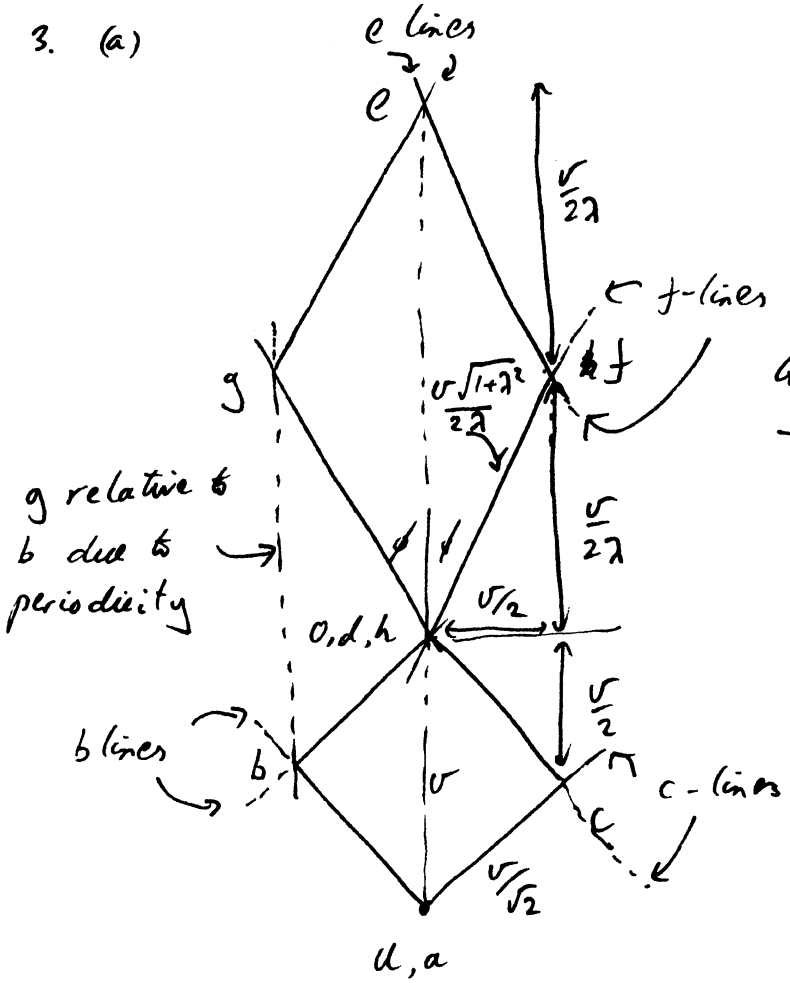

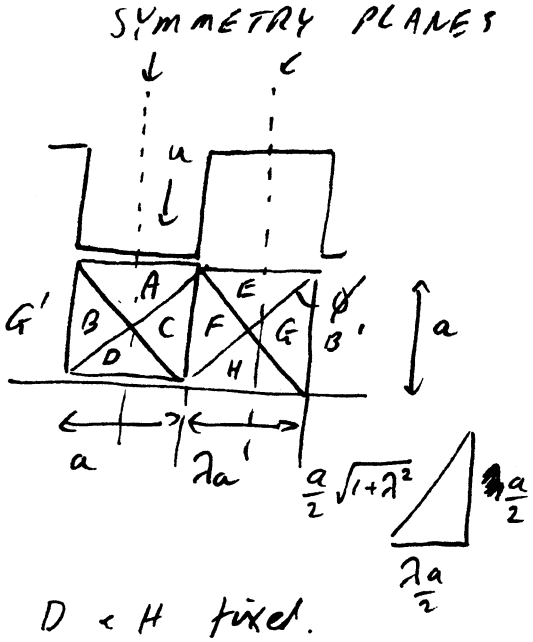

D < H fixed.

Check volume constancy

$v_e \cdot \lambda a + v_a \cdot a = 0$ ✓

(b) Work in = power dissipated = $\Sigma k l \Delta v$ (per unit d

Easiest to use part of model between symmetry planes shown abo

$p \cdot v \frac{a}{2}(1+\lambda) = k\,(A/C + C/D + C/F + F/E + F/H)$

[Alternatively use all blocks shown: $pa(1+\lambda) = k\,(A/C + C/D + A/B + B/D + E/F + F$
$+ H/G + E/G + \underbrace{\tfrac{1}{2}BG' + \tfrac{1}{2}GB'}$,
share contribution at edge of model

Use symmetry $A/C = C/D$, $E/F = F/H$)

$$p\frac{a(1+\lambda)}{2k}v = 2\frac{a}{\sqrt{2}}\frac{v}{\sqrt{2}} + 2v\,a\frac{\left(\sqrt{1+\lambda^2}\right)^2}{2\times 2\lambda} + a\frac{v}{2}\left(1+\frac{1}{\lambda}\right)$$

(A/C, F/E, C/F)

$$p = \frac{2k}{1+\lambda}\left(1 + \frac{1}{2}\left(\frac{1+\lambda^2}{\lambda}\right) + \frac{1}{2} + \frac{1}{2\lambda}\right)$$

$$= \frac{k}{\lambda(1+\lambda)}\left(3\lambda + \lambda^2 + 2\right)$$

Examiner's Tip: Don't jump to the answer via a 'wild' last step. Be honest!

3(c)(i) $\lambda \ll 1$ $\quad \frac{p}{k} \sim \frac{2}{\lambda} \xrightarrow[\lambda \to 0]{} \infty$

(ii) $\lambda \gg 1$ $\quad \frac{p}{k} \sim 1$

For $\lambda \ll 1$

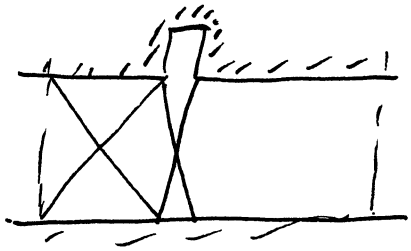

assumed deformation mode extends to bottom. Expect a more localised field (like back extrusion), so a poor estimate is expected, overestimating the load.

[Back extrusion
Lower bound $p = 2k \ln \frac{1}{\lambda}$]

For $\lambda \gg 1$

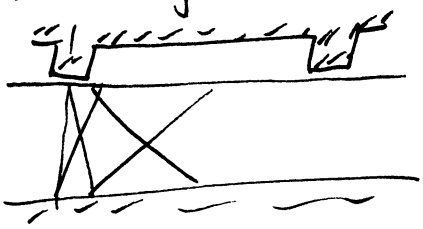

Now like indentation:

$p \frac{a}{a(1+\lambda)} \simeq 6k \Rightarrow \frac{p}{k} \sim \frac{6}{\lambda}$

The assumed field extends the deformation too far from the load point and also gives a poor estimate.

3(d) Choose process appropriate to copper.

Easiest rolling with grooved rolls:

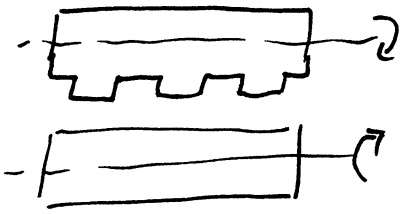

Also extrusion.

Reduce loads by hot forming or lubrication.

[The hodograph was incorrect in more than half solutions. Some information about the periodicity/symmetry of the problem needs to be brought in. The idea of the plastic work upper-bound model was clear to most candidates, but then not using symmetry made the working very long. Similarly some thinking about what to do with the edges of the problem need to be addressed. Very few made sensible comments about the appropriateness of the proposed velocity field for extreme geometries (part c), though there were many good alternative forming processes in (d).]

4 (a) (i)
Ferritic steels (bcc structure) undergo a transition from high-temperature ductile behaviour to low-temperature brittle behaviour because the yield stress rises as the temperature falls. Dislocation mobility in bcc materials (which are not close-packed) is thermally activated, so mobility falls as the temperature drops until some slip systems are quenched out. The ductile-brittle transition occurs when the equivalent stress to cause yielding σ_e rises above the fracture stress σ_f.

The temperature at which the transition occurs depends on the specimen geometry. There is an enhanced stress and reduced ductility at crack tips in thick specimens (due to the plane strain constraint at the tip of the crack). This plane strain constraint is due to the surrounding elastic material, which means that a higher effective stress $2.5\sigma_y$ is needed to get plastic deformation at the crack tip as compared with plane stress or uniaxial stress, where the effective stress is equal to the yield stress σ_y [in a similar way to the constraint found in a hardness tests, causing a $\times 3$ increase in stress for indentation as compared with uniaxial tension).] The effect of temperature on effective stress at the crack tip is seen in the left hand sketch below. The ductile-brittle transition occurs when the failure stress exceeds the yield stress, so that the transition occurs at a higher temperature in thick specimens (plane strain) than in thin ones (plane stress), as sketched in the right hand figure.

Austenetic steels have an fcc structure which does not suffer from such a temperature-dependant yield stress.

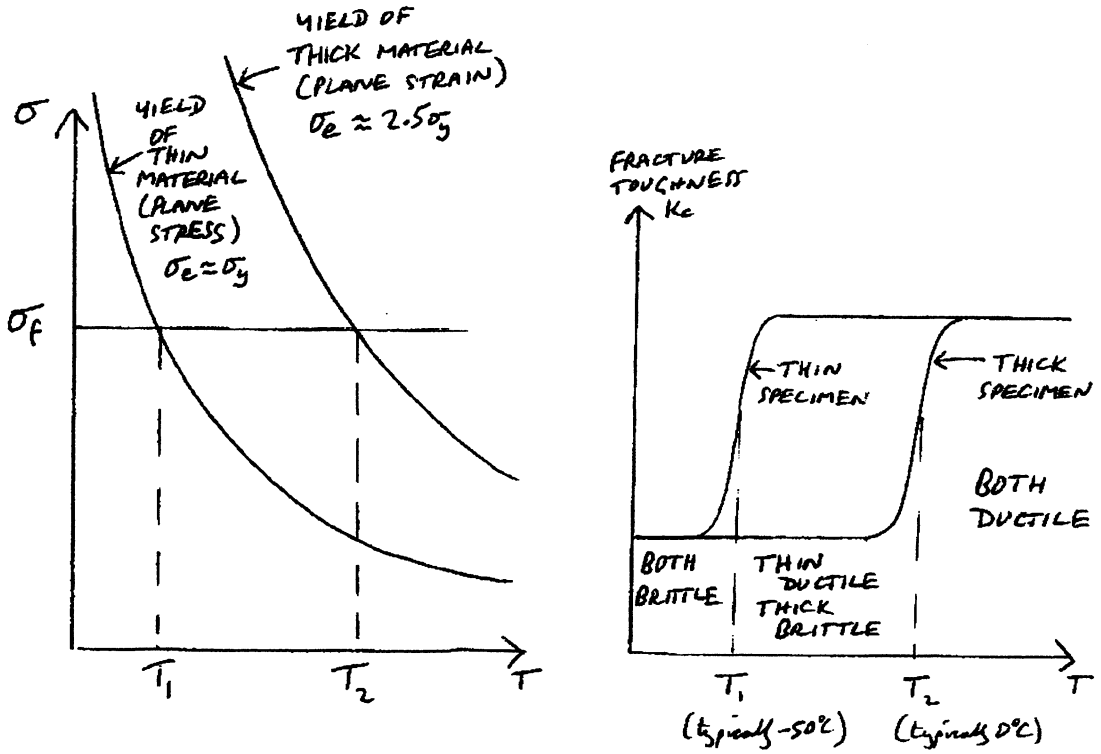

4 (a) (ii) Un-notched samples still show the transition, but at lower temperatures. The presence of cracks or notches increases the local stress and so introduces additional plastic constraint. It is this increase in local stress which pushes the transition to higher temperatures for notched specimens.

Cold-deformation increases the yield stress of the material, but does not affect the fracture stress. The effect is to shift the yield stress curves in part (i) upwards, so they intersect the fracture stress curve at higher temperatures. Cold-deformation therefore increases the transition temperatures.

4 (b) (i) Thin specimens failing under plane stress conditions: large-scale ductility and necking. **Thick specimens** (failing under plane strain conditions) show very little plastic deformation, with planar fracture surfaces, no necking. Shear lips will be found at the edges, where plane stress conditions take over, but these do not form an appreciable fraction of the total crack. The plane strain region is not proper brittle fracture because micro-ductility still occurs (crack-tip process zone diameters smaller by a factor of one third than in plane stress). The facets typical of brittle fracture are not found. The apparently brittle fracture goes with a stress intensity factor K which is lower by a factor of 2.5 than that associated with the ductile fracture.

Very thin specimens

The stress intensity factor drops off as the specimens become thinner (process zone reduces in size with the thickness). Thin metal sheet often fails by a low-energy mode involving out-of-plane tearing (mode III). Dislocations can run all the way through the sheet, so there are no work-hardening effects. The material fails by shearing along planes of maximum shear stress, and the process zone size drops to nearly zero.

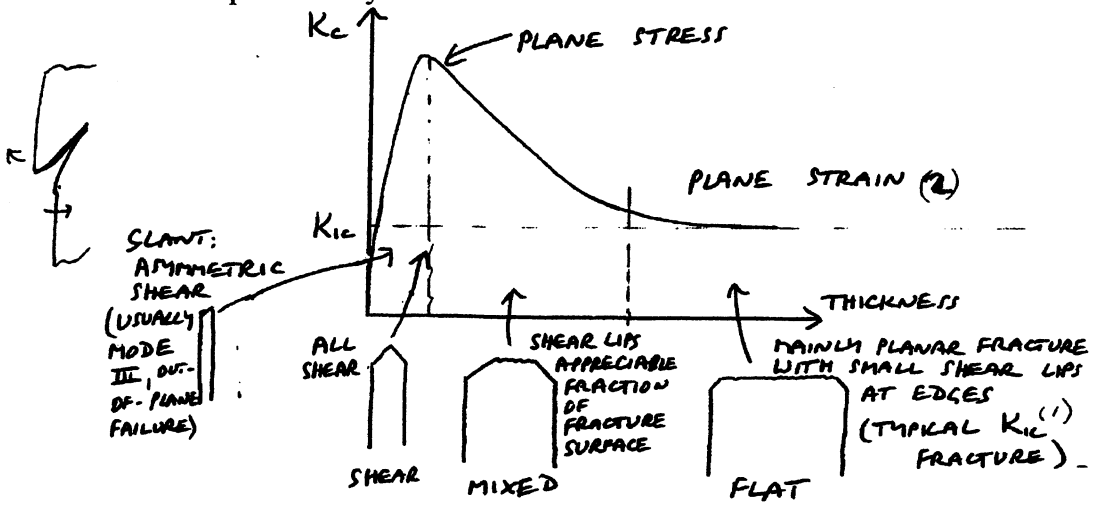

4 (b) (ii) Polymers do not in general suffer out-of-plane tearing, so the fracture toughness does not drop off with very thin specimens. The specimen thickness at which polymer fracture behaviour changes from the high-energy, ductile fracture typical of thin specimens to the more brittle behaviour typical of thick specimens is typically when the thickness gets above $2\,(K_{IC}/\sigma_y)^2$.

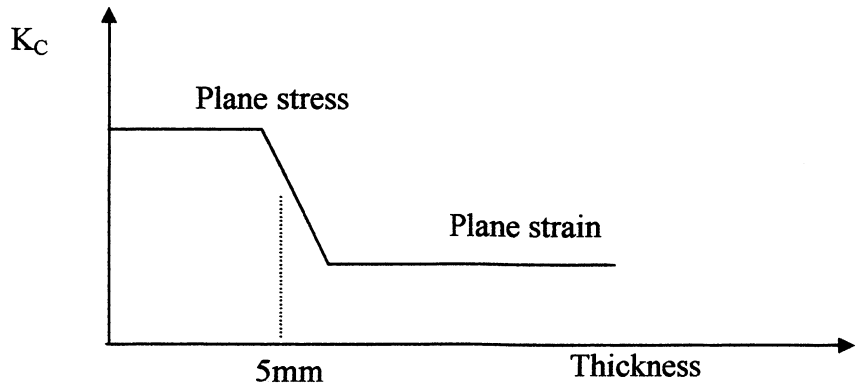

[Vagueness on the reasons for the increase in effective yield strength in thick notched samples (or missing this point completely), and hence difficultly explaining the effect of thickness on transition temperature effectively. The difference between austenitic and ferritic steels was not normally identified. Very few people were able to apply their ideas from (a)(i) to explain the differences associated with notches or cold-forming on the transition temperature. There were general comments about stress concentration with notches, or increased dislocation density with cold working but these observations were not related to the change in transition temperature. Part (b) was done well.]